A Kinetic Study of Oxidation of Praseodymium Oxides: $PrO_{1.714} + 0.032\ O_2 \rightarrow PrO_{1.778}$*

H. INABA,†, S. P. PACK, S. H. LIN, AND L. EYRING‡

Department of Chemistry, and Center for Solid State Science, Arizona State University, Tempe, Arizona 85281

Kinetic and thermodynamic studies between the ι ($n = 7$) and the ζ ($n = 9$) phases of the homologous series of the praseodymium oxides (Pr_nO_{2n-2}) have been carried out as a function of oxygen pressure at 535, 540, 550, and 570°C. The thermodynamic study was carried out by measuring the weight of the oxide sample at equilibrium at these temperatures as a function of pressure. The existence of a reproducible hysteresis loop which depends on the temperature and pressure is shown. The kinetic study was carried out by measuring the weight change of the sample as a function of time after a sudden increase of oxygen pressure initiated the reaction. In order to interpret the kinetic data, various theoretical models assumed, for example, to depend upon diffusion, a moving boundary, a phase boundary reaction control, or nucleation and growth have been examined. None of these models, however, is capable of correlating the experimental data. It was found that for the powder sample diffusion of oxygen is much faster than the rate of reaction and the reaction kinetics is first order with respect to both the concentration of reactant and the ambient oxygen pressure. A linear plot of the reaction rate versus the ambient pressure extrapolates to a finite pressure at zero rate, suggesting that the reaction does not begin until this pressure is attained. It has been shown that this pressure corresponds to the minimum required to produce ζ phase as shown by the isothermal hysteresis loop along the oxidation path. From the measurements of the oxygen pressure and temperature dependence of the observed rate constants, the activation energy of the reaction was determined to be 45.3 kcal/mole.

1. Introduction

The praseodymium oxides belong to a fluorite-related homologous series R_nO_{2n-2} ($n = 4, 6, 7, 9, 10, 11, 12, \infty$) of intermediate phases with well-defined stoichiometries and ordered structures (*1, 2*). The thermodynamic studies of phase transformations

between these intermediate phases have shown that reproducible hysteresis loops are found when the phase reaction cycle is completed between two phases (*3–10*). The causes of chemical hysteresis are far from understood in spite of its frequent occurrence in chemical systems. In a previous paper (*10*), a thermodynamic model of hysteresis based on the regular solution theory was developed by invoking metastabilities. It was applied to the observed hysteresis for the phase reactions $Tb_7O_{12} \leftrightarrows (7/2)Tb_2O_3 + (3/4)O_2$ and $Pr_9O_{16} \leftrightarrows (9/7)Pr_7O_{12} + (2/7)O_2$. However, the model

295

can only provide the gross features of the hysteresis loop between two phases. It cannot account for the fact that constant-temperature (or constant pressure) regions are never observed in the hysteresis loops associated with the rare earth oxide systems or that scanning loops are observed in these systems.

In order to understand the nature and mechanism of hysteresis it is necessary to have detailed knowledge of the structural and thermodynamic relationships of the end members of the phase reaction and of their intergrowth kinetics. In this paper, we shall report kinetic and thermodynamic studies of the phase reaction: ι ($PrO_{1.714}$, $n = 7$ in R_nO_{2n-2}) + 0.032 $O_2 \rightarrow \zeta$ ($PrO_{1.778}$, $n = 9$ in R_nO_{2n-2}). It will also be shown that the kinetics data should be interpreted using information from the oxidation path of the hysteresis loop. The ι phase has a rhombohedral structure with $a = 6.750$ Å and the ζ phase has a triclinic structure with $a = c = 6.5$ Å, and $b = 8.4$ Å (1). Both phases have common a and c axes, but the length of the b axis of the unit cell differs by a factor of 9/7 between the two phases. The development of intergrowth of ι in ζ phase has been observed by high-resolution electron microscopy. However, due to the low ambient oxygen pressure it has not yet been possible to observe the oxidative phase reaction $\iota \rightarrow \zeta$ under the electron microscope.

The experimental results of the kinetic study for the phase reaction $\iota \rightarrow \zeta$ have been fit to three existing theoretical models: (i) diffusion control (11), (ii) moving boundary or phase boundary reaction control (12, 13), and (iii) nucleation and growth control (14). Since these models do not fit the experimental results, a new model is proposed for the phase reaction.

2. Experimental

Kinetic and thermodynamic measure-

ments of the phase reaction

$$Pr_7O_{12}(s) + (2/9)O_2(g) \leftrightarrows (7/9)Pr_9O_{16}(s)$$

have been carried out on powdered and single-crystal specimens.

The praseodymium oxide powder was of 99.999% purity, furnished by the Research Chemical Division of Nucor Corporation. The crystals were grown by the hydrothermal method (15) and sized with Tylor series sieves to get an average size of 0.07 mm in diameter. The oxygen was supplied by the Liquid Air Company with stated purity of 99.9% and was used without further purification.

For the kinetic runs on powders an Ainsworth balance was used. About 1.45 g of $PrO_{1.714}$ was spread evenly in four platinum dishes held one above the other to assure rapid and even access to the oxygen atmosphere. Each dish was 1.6 cm in diameter and 0.5 cm in height with a stacked spacing of 0.3 cm.

The irreproducibility in the weight measurement for each run was within ± 20 μg. The inaccuracy in the weight including irreproducibility among runs and the error in the correction for the TMF (thermal molecular flow) (16) effect was ± 100 μg, corresponding to a compositional error of ± 0.0007 in the oxygen/metal ratio.

The kinetic measurements on single crystals were made on a Cahn RG thermobalance. About 90 mg of $PrO_{1.714}$ crystals were placed in a platinum bucket 1.0 cm in height and 0.3 cm in diameter. The irreproducibility and inaccuracy of the weight measurements was about ± 5 and ± 20 μg, corresponding to a compositional error of ± 0.0023 in the oxygen/metal ratio.

The system was calibrated to determine the effect of the TMF as a function of pressure at the experimental temperatures, using oxygen without the sample and argon with the sample. The largest TMF corrections made in the data analysis were 1.2 mg

in the Ainsworth system and 80 μg in the Cahn system.

In both systems, the sample weight, temperature, and ambient oxygen pressure were read directly by a PDP-8 computer. The temperature was maintained constant within ±1°C using an RI 624 Thermac controller and was measured using a Pt/Pt + 10% Rh thermocouple located in the quartz reaction tube about 0.5 cm below the platinum sample bucket. The pressure was monitored by a Datametrics Model 1014A capacitance manometer within ±0.05 Torr accuracy.

In the thermodynamic (hysteresis) study, the sample was kept at the temperature desired and a reduced pressure (as low as 0.1 Torr) for more than 10 hr to ensure the production of ι phase. The oxygen was then admitted and the weight change was observed until equilibrium was attained. It took a rather short time (ca. 20 min) in the nonstoichiometric regions of ι or ζ phase, but a long time (from 2 to 16 hr) in the hysteresis regions.

In the kinetic runs, the sample was heated at 700°C for more than 30 min under an oxygen pressure of less than 10 Torr to ensure the complete reduction to ι phase. The pressure in the reaction chamber was finally adjusted to 0.25 Torr at the desired experimental temperature and the system was allowed to attain equilibrium. The desired initial pressure (typically 4.25 Torr) was obtained by opening a valve to a ballast where the oxygen pressure was higher than that in the reaction chamber. The pressure decreased by about 0.1 Torr as the reaction proceeded to its final value which was reported as the reaction pressure. These kinetic runs were made as a function of pressure at a series of temperatures. The temperature, pressure, and weight were measured 1000 times consecutively in 0.5- to 8-sec intervals using the PDP-8 computer. The final values were taken 0.5–8 hr later when the reaction was complete.
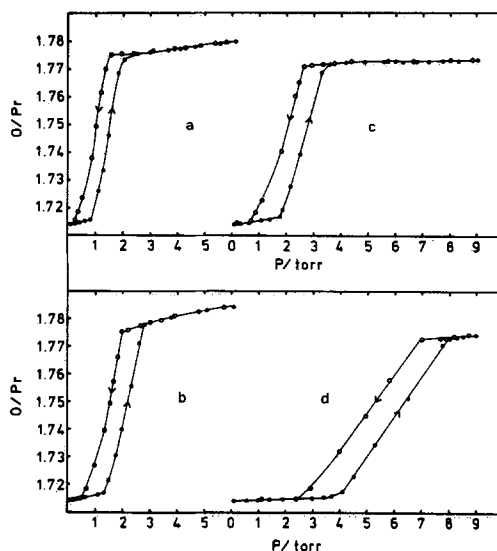

FIG. 1. Isothermal hysteresis loops between ι and ζ phases: (a) 535°C; (b) 540°C; (c) 550°C; (d) 570°C. ●, oxidation; ○, reduction.

3. Results

3.1. The Hysteresis Study

An isothermal hysteresis study has been carried out between the ι and the ζ phase for a powder sample at different temperatures by changing the pressure. The results are shown in Fig. 1.

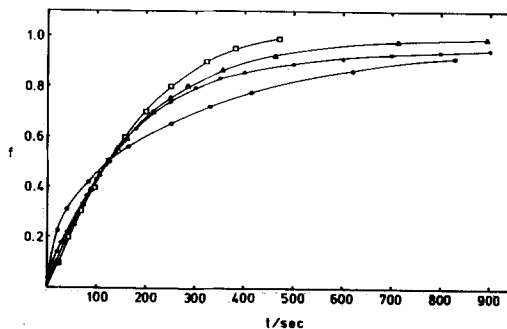The composition of the praseodymium oxides were not determined absolutely,

FIG. 2. A typical kinetic run for a powder sample at 550°C and 4.14 Torr. The fraction of reaction is plotted against time: ●, observed; ○, $f = 1 - (6/\pi^2)$ $\sum_n (1/n^2) \exp(-n^2 D^* t)$; □, $f = 1 - (1 - kt)^3$; △, $f = 1 - \exp(-kt)$.

rather the O/Pr ratio at a pressure of 0.1 Torr was set as 1.714 on the basis of previous experience. The features of the hysteresis curves are similar to those obtained in the isobaric studies (*10*). The complete loop is symmetrical with respect to the ι and ζ phases but shifts to higher pressures and increases in width as the temperature increases.

3.2. The Kinetic Study

A kinetic run for a powdered sample at 550°C and a final pressure of 4.14 Torr is shown as a typical example in Fig. 2, where the weight fraction, *f*, of the sample is plotted against time. The weight fraction is defined as

$$f = \frac{W_t - W_i}{W_f - W_i}, \tag{1}$$

where W_f, W_i, and W_t are the final weight, the initial weight, and the weight at the time *t*. The half-reaction time, $t_{1/2}$, for these measurements is shown as a function of pressure, *P*, in Fig. 3. The function of *P* decreases inversely with $t_{1/2}$, approaching a limiting pressure depending upon the temperature. Thus the reaction rate *U* (defined
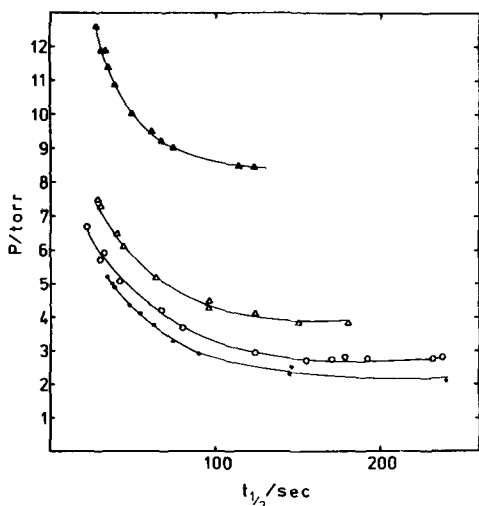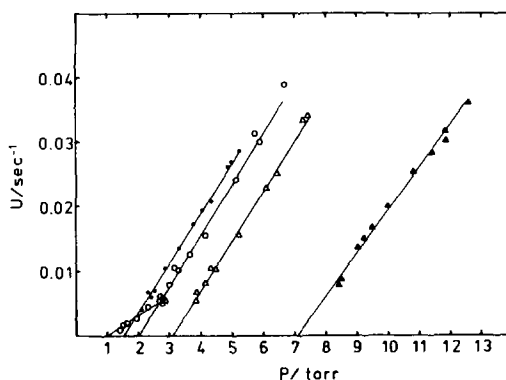
Fig. 4. The reaction rate *U* vs reaction pressure: ●, 535°C; ○, 540°C; ▲, 550°C; △, 570°C.

as the inverse of $t_{1/2}$) plotted against *P*, as in Fig. 4, is linear. These lines extrapolate to zero rate at some pressure different from the reaction pressure depending upon the temperature. (Notice that below a certain pressure at 540°C the reaction rate deviates from the line drawn. This will be discussed below.)

A series of kinetic runs at one temperature has been made for the single-crystal sample. A typical run, shown in Fig. 5, is similar to that of a powder sample. The
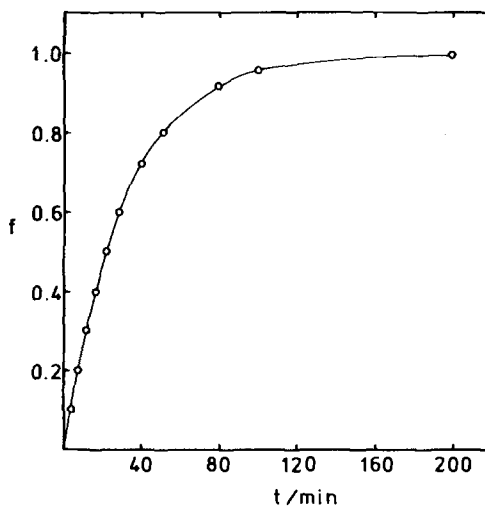
Fig. 3. The half-reaction time vs reaction pressure: ●, 535°C; ○, 540°C; ▲, 550°C; △, 570°C.

Fig. 5. A typical kinetic run for a single-crystal sample. The fraction of reaction is plotted against time.

reaction rate U at 535°C is plotted against pressure in Fig. 6. In this case as with powder the linear extrapolation to zero rate gives a finite pressure. The magnitude of U for a single-crystal specimen is less than that of a powder sample at 535°C by a factor of 35, as seen by comparing Figs. 4 and 6.

4. Discussion

The kinetics of physicochemical transitions or reactions in solids may consist of several simple physical and chemical "elementary" processes involving, for example, movement of a particle of matter, changes in structure, physical state, or chemical composition. In the experimental measurements described above, only information about the weight change of the sample as a function of time at a particular temperature and pressure is obtained. Thus, in order to find rate constants which reflect the elementary processes associated with the phase reaction of praseodymium oxide, the experimental data must be fitted to a particular kinetic model. Most of the models for solid state reactions proposed by others have been compiled and solved (17). In this study, several plausible models were tried in fitting the experimental data
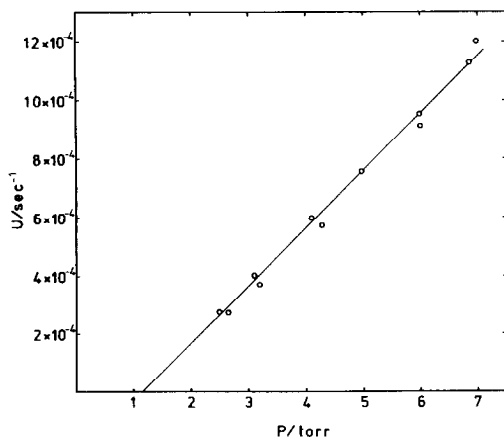
FIG. 6. The reaction rate U for single crystals vs reaction pressure at 535°C.

including simple diffusion, moving boundary, phase boundary reaction control, and nucleation and growth.

According to the simple diffusion model, the weight change observed is controlled by the diffusion of an absorbed species. In this case, the diffusion equation

$$\frac{\partial c}{\partial t} = D \nabla^2 C \qquad (2)$$

must be solved subject to appropriate boundary conditions. For a spherically symmetric system, with a constant diffusion coefficient, the fraction of weight change f is given by (11)

$$f = 1 - \frac{6}{\pi^2} \sum_{n=1}^{\infty} \frac{1}{n^2} \exp(-n^2 D^* t), \qquad (3)$$

where $D^* = \pi^2 D / r_0^2$.

In Fig. 2 the simple diffusion model of Eq. (3) is plotted by fitting the curve at $f = 0.5$ (i.e., $t = t_{1/2}$) using the results for the powder sample. The fit is unsatisfactory.

Actually, a fit according to this model should not be expected for two reasons. First, the diffusion constant of oxygen in ζ-phase praseodymium oxide has been measured by Fox as reported by Eyring et al. (18) (Table I). Under our experimental conditions, it ranges from 2×10^{-10} to 25×10^{-10} cm²/sec. For example, if we choose 10^{-9} cm²/sec for the diffusion constant in the ζ phase at 535°C, and use 0.07 mm and 0.5 μm as the diameters of the single crystal and the powder particle, respectively, D^* is calculated to be 8×10^{-4} and 9 sec⁻¹ for the single-crystal sample and the powder sample, respectively. These values can be compared with the reaction rate U obtained experimentally. It can be seen that the 8×10^{-4} sec⁻¹ value is comparable to the reaction rate U for the single-crystal sample (see Fig. 6), but the 9 sec⁻¹ value is much larger than the reaction rate U for the powder sample (see Fig. 4).

Second, in terms of point defects oxygen

TABLE I

DIFFUSION CONSTANT OF POWDERED SAMPLE, ζ PHASE: RESULTS FOR
$PrO_{1.778}$

Run	Pressure (mm Hg)	Temperature (°C)	Average slope ($\times 10^5$)	D ($\times 10^{19}$)
1	5.40	511.5	0.44	0.75
2	6.00	509.8	2.7	9.7
3	6.02	478.5	1.7	6.4
4	9.13	525.2	0.88	2.1
5	8.49	542.2	8.4	25
6	8.60	558.9	29	180
7	7.17	574.9	0.94	1.8

diffusion in the praseodymium oxide has been shown to take place via oxygen vacancies and/or interstitials. Rao and Rao (19) measured the electrical conductivity of PrO_x below 700°C and found its pressure dependence to change from $P_{O_2}^{1/6}$ to $P_{O_2}^{-1/2}$ as the composition varies from $PrO_{1.5}$ to PrO_2, with a maximum occurring at $PrO_{1.75}$. Taking into account all the possible types of defects, Lau et al. (20) have proposed the following expression to explain the observed pressure dependence of the diffusion constant in the ι phase,

$$D = \alpha_1 P_{O_2}^{1/2} + \alpha_2 P_{O_2}^{1/6}$$
$$+ \alpha_3 P_{O_2}^{-1/6} + \alpha_4 P_{O_2}^{-1/2}. \quad (4)$$

Obviously this expression cannot explain the linear pressure dependence of the reaction rate U shown in Fig. 4.

We should also compare the pressure dependence of the diffusion coefficient of the ζ phase with that of the reaction rate U; however, no such experimental data are available. We conclude that the simple diffusion model is not followed by the phase reaction $\iota \rightarrow \zeta$ in the PrO_x–O_2 system.

Next, the so-called moving boundary mechanism is considered. According to this model, the reaction takes place on the boundary between the product and the reactant and the thickness of the product layer is changing with time. For a spherically symmetric system, the model has

been solved only when the steady state approximation has been used (12).

In this case, the expression for f is given by

$$Kt = R[1 - (1 - f)^{1/3}]$$
$$+ \frac{1}{2} - \frac{1}{2}(1 - f)^{2/3} - \frac{1}{3}f, \quad (5)$$

where $R = D/kr_0$ and $K = D(C^* - C_{eq})/d_0r_0^2$. Here d_0 represents the density of the reactant and C_{eq} is the equilibrium concentration. Notice that in this case when $f = 1$, $t = (R + \frac{1}{6})/K$. This differs from the model presented above (see Eq. (3)) and those to be given below (see Eqs. (7) and (17) or (19)) where as $f \rightarrow 1$, $t \rightarrow \infty$. This type of solution has been widely used in the kinetic study of, for example, the reduction of iron oxides and the oxidation of nickel (12, 21). For powders, diffusion is much faster than the reaction rate, hence R in Eq. (5) becomes very large. Under these conditions we obtain the so-called phase boundary reaction-controlled model

$$f = 1 - (1 - kt)^3. \quad (6)$$

Equation (6) can be obtained from Eq. (5) by letting $R \rightarrow \infty$; in this case $k = K/R$. Notice that at $kt = 1, f = 1$. In the PrO_x–O_2 system it has been fit satisfactorily to the reaction $Pr_6O_{11} + \frac{1}{2}O_2 \rightleftarrows 6PrO_2$ (13).

The plot of Eq. (6) is compared with the experimental results in Fig. 2. The theoretical curve is chosen to fit the experimental

plot at $f = 0.5$. It is clear that agreement between theory and experiment is not good.

Another plausible model frequently employed to fit experimental data is that of nucleation and growth. For grain boundary nucleation (plate-like growth), Cahn (*14*) has shown that in the long-time limit f can be expressed as

$$f = 1 - \exp(-2SGt), \qquad (7)$$

where S represents the boundary area per unit volume and G represents a constant growth rate. This model cannot explain our experimental results since df/dt would equal zero at $t = 0$, while the data show that df/dt is finite at $t = 0$. At large t, Eq. (7) does not satisfactorily fit our data, although it does fit well in the middle region (see Fig. 2). Finally, it is difficult to explain why G should vary linearly with P and approach zero at a finite oxygen pressure.

As is suggested by the above discussion, the existing models of solid state reactions cannot be used to interpret these experimental results. Before proceeding to develop a new model we summarize the main features of the experimental findings of the kinetics for the phase reaction, $\iota \to \zeta$. For the powdered sample, diffusion of oxygen is much faster than the reaction. The reaction rate U measured by the inverse half-
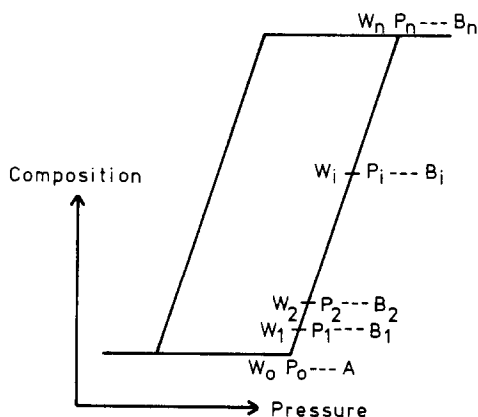

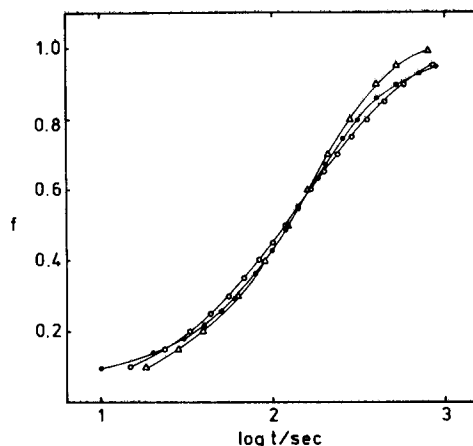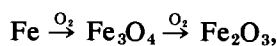
FIG. 8. Experimental and theoretical fits of f vs log t at 550°C and 4.14 Torr ($P > P_n$). ●, observed; ○, $[\beta'(1 - f)/\beta' - f] = \exp[-k'(P - P_n)t]$, $\beta = 1.451$; △, $f = 1 - \exp(-kt)$.

lifetime varies linearly with the oxygen pressure with a finite intercept, and df/dt is not zero at $t = 0$.

In the system, where reproducible hysteresis is observed, the Gibbs free energy is expressed by factors (*8*) other than temperature, pressure, and composition that might affect a phase transformation, e.g., surface energy or distribution of domains. Consequently, the phase rule must include extra terms,

$$F = C - P + 2 + \Sigma\pi.$$

In this sense we have many "intermediate phases" along the hysteresis loop. An idealized isothermal hysteresis loop representing the phase reaction is shown in Fig. 7 in the shape of a parallelogram. The original phase (ι in this case) is represented by A and B_1, B_2,---B_n represents an arbitrary series of intermediate compositions. The corresponding equilibrium pressures are indicated by P_1, P_2,---P_n. As in the case of the isothermal oxidation of Fe (*22*) and UC (*23*),

$$Fe \xrightarrow{O_2} Fe_3O_4 \xrightarrow{O_2} Fe_2O_3,$$

$$UC \xrightarrow{O_2} UO_2 \xrightarrow{O_2} U_3O_8,$$

FIG. 7. An idealized isothermal hysteresis loop.

we shall assume that the phase reaction,

$$\iota \xrightarrow{O_2} \zeta, \qquad (8)$$

also passes through the path of the intermediate phases B_1, B_2, --- B_n.

From Eq. (8) and the fact that U varies linearly with the oxygen pressure, we write the rate expression for the phase reaction as

$$-\frac{dA}{dt} = k'A(P - P_i), \qquad (9)$$

where A is now the concentration of the initial phase, k' is the rate constant, P is the ambient pressure, and P_i is the equilibrium pressure of the intermediate phase (see Fig. 7). The term $(P - P_i)$ in Eq. (9) means that the reaction does not proceed until the ambient pressure P reaches P_i, the equilibrium pressure of the intermediate phase.

In order to convert this rate expression into a rate equation expressed in terms of the weight fraction, f, we introduce the weight of the sample W,

$$W = V(AM_A + BM_B), \qquad (10)$$

where V is the volume of the sample, B is the concentration of the product, and M_A and M_B represent the molecular weights of A and B, respectively. At time zero and infinity, we have

$$W_0 = VA_0M_A \qquad (11)$$

and

$$W_\infty = V(A_\infty M_A + B_\infty M_B), \qquad (12)$$

respectively.

Noticing that

$$A + B = A_\infty + B_\infty = A_0, \qquad (13)$$

we obtain

$$f = \frac{W - W_0}{W_\infty - W_0} = \frac{A_0 - A}{A_0 - A_\infty}. \qquad (14)$$

Substituting Eq. (14) into Eq. (9) yields

$$\frac{df}{dt} = k'\frac{A_0}{A_0 - A_\infty} - f(P - P_i). \qquad (15)$$

Since we assume that the oxidation branch of the hysteresis loop is linear against pressure (see Fig. 7), we have $P_i = P_0 + f(P_n - P_0)$. When P is greater than P_n in Fig. 7, the system becomes ζ phase completely, hence $A_\infty = 0$; in this case Eq. (15) becomes

$$\frac{df}{dt} = k'(1 - f)[P - P_0 - f(P_n - P_0)], \qquad (16)$$

which can easily be integrated as

$$\frac{\beta(1 - f)}{\beta - f} = \exp[-k'(P - P_n)t], \qquad (17)$$

where $\beta = (P - P_0)/(P_n - P_0)$. On the other hand, when P is smaller than P_n, $A_\infty \neq 0$ and $P_i = P_0 + (P - P_0)f$. Substituting this relation into Eq. (15) yields

$$\frac{df}{dt} = k'(P - P_0)(1 - f)\frac{(A_0 - f)}{A_0 - A_\infty}, \qquad (18)$$

which can be integrated as

$$\frac{\beta'(1 - f)}{\beta' - f} = \exp[-k'(P - P_0)(\beta' - 1)t], \qquad (19)$$

where $\beta' = A_0/(A_0 - A_\infty)$.

Consider an energy level versus reaction coordinate diagram; notice that the initial energy level is dependent on P_0 because the phase reaction does not proceed until this
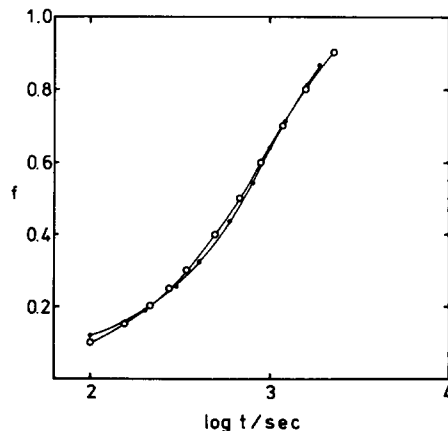

FIG. 9. Experimental and theoretical fits of f vs log t at 540°C and 1.44 Torr ($P < P_n$). ●, observed; ○, $[\beta'(1 - f)/\beta' - f] = \exp[-k'(P - P_0)(\beta' - 1)t]$.
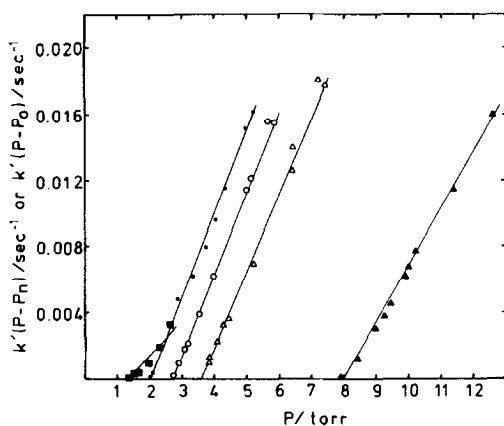
FIG. 10. Plots of $k'(P - P_n)$ and $k'(P - P_0)$ vs pressure. $k'(P - P_n)$: ●, 535°C; ○, 540°C; △, 550°C; ▲, 570°C. $k'(P - P_0)$: ■, 540°C.

pressure is reached. P_0 should depend on temperature as can be seen from Fig. 1. In other words, k' may depend on temperature through P_0; this is the reason the slopes of the curves $k'(P - P_n)$ vs P decreases with T (see Fig. 10). The dependence of k' on P_0 can be taken into account by shifting the energy of the initial state by the amount, $RT \ln P_0$, i.e.,

$$k' = k \exp \frac{(-RT \ln P_0)}{RT} = \frac{k}{P_0}. \quad (20)$$

The expression for $U = t_{1/2}^{-1}$ can be obtained from Eqs. (17) and (19) as

$$U = \frac{k'(P - P_n)}{\ln(2\beta - 1/\beta)} \quad (21)$$

and

$$U = \frac{k'(P - P_0)(\beta' - 1)}{\ln(2\beta' - 1/\beta')}, \quad (22)$$

respectively.

In Figs. 8 and 9 we show the application of Eqs. (17) and (19) to fit the experimental results, where P_n and P_0 are taken from the observed hysteresis curves of Fig. 1. As can be seen from these figures the agreement between theory and experiment is satisfactory. For the case where $P > P_n$, the observed $k'(P - P_n)$ obtained from the
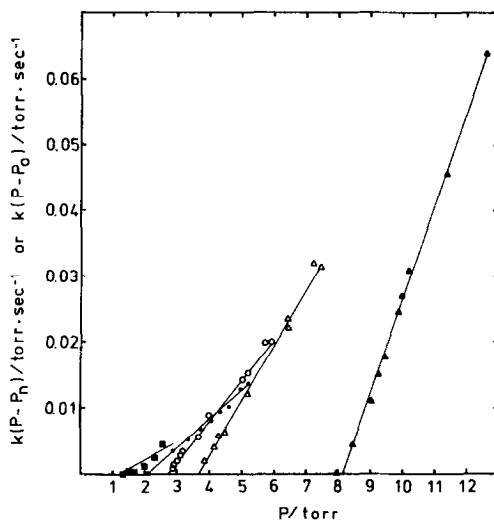

FIG. 11. Plots of $k(P - P_n)$ and $k(P - P_0)$ vs pressure. $k(P - P_n)$: ●, 535°C; ○, 540°C; △, 550°C; ▲, 570°C. $k(P - P_0)$: ■, 540°C.

use of Eq. (21) is plotted (Fig. 10) against the ambient pressure at different temperatures. A good linear relationship does exist in each case and the straight lines intersect at P_n as predicted by the theoretical model. Similarly a plot for the case of $P < P_n$ is also shown in Fig. 10, and a good linear relationship is found with an intercept at P_0 predicted by the theory.

Using Eq. (20), we get $k(P - P_n)$ and $k(P - P_0)$ which when plotted against
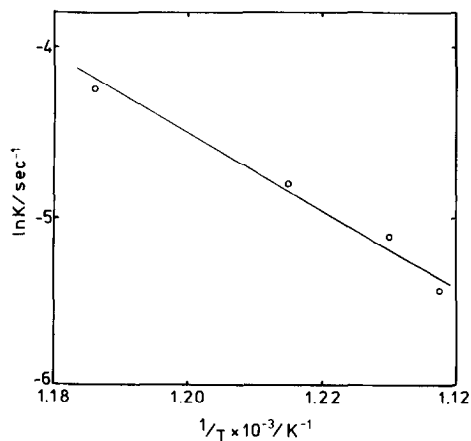

FIG. 12. A plot of $\ln k$ vs $1/T$.

pressure as shown in Fig. 11, give lines whose slopes increase with temperature. From the slopes of the straight lines we can determine k as a function of temperature. A plot of $\ln k$ vs $1/T$ is shown in Fig. 12 from which an activation energy of 45.3 kcal/mole is obtained.

In concluding this discussion we point out that the reaction rate depends on the oxidation branch of the hysteresis loop, since the driving force of the reaction is proportional to $(P - P_i)$ where P_i is the actual equilibrium pressure of the reacting material. The rate equation depends upon the ambient pressure P whether or not it is greater than P_n. The extrapolated pressure at which the rate is zero does depend upon whether P is greater or less than P_n but the mechanism for powder samples appears to be the same regardless of the pressure.

Furthermore, control of the particle size of the specimen makes possible elimination of the diffusion effect as in the case of the powder sample. This suggests that just as the diffusion effect may be taken from consideration in specimens of sufficiently small particle size a kinetic study of larger crystallites can be used to determine the diffusion coefficient since in this case both diffusion and reaction would contribute to the rate of reaction.

This phenomenological treatment of the phase reaction, ι to ζ, in the oxidation of a praseodymium oxide points to those environmental factors which affect the mechanism of reaction and hence determine its rate. Already, however, information on the mechanism at nearly atomic resolution is being provided by examining specimens, quenched in the course of reaction, by high-resolution electron microscopy (to be published separately). The next step will be to use these suggestions to formulate and test the detailed mechanism of this reaction involving materials having extended defects.

References

1. P. KUNZMANN AND L. EYRING, *J. Solid State Chem.* **14**, 229 (1975).
2. R. T. TUENGE AND L. EYRING, *J. Solid State Chem.*, in press.
3. B. G. HYDE, D. J. M. BEVAN, AND L. EYRING, *Phil. Trans. Roy. Soc. London Ser. A* **259**, 583 (1966).
4. D. A. BURNHAM AND L. EYRING, *J. Phys. Chem.* **72**, 4415 (1968).
5. D. A. BURNHAM, L. EYRING, AND J. KORDIS, *J. Phys. Chem.* **72**, 4424 (1968).
6. J. KORDIS AND L. EYRING, *J. Phys. Chem.* **72**, 2044 (1968).
7. R. P. TURCOTTE, M. S. JENKINS, AND L. EYRING, *J. Solid State Chem.* **7**, 454 (1973).
8. A. T. LOWE AND L. EYRING, *J. Solid State Chem.* **14**, 383 (1975).
9. A. LOWE, K. H. LAU, AND L. EYRING, *J. Solid State Chem.* **15**, 9 (1975).
10. D. R. KNITTEL, S. P. PACK, S. H. LIN, AND L. EYRING, *J. Chem. Phys.* **67**, 134 (1977).
11. B. SERIN AND R. T. ELLICKSON, *J. Chem. Phys.* **9**, 742 (1941).
12. B. SETH AND H. ROSS, *Trans. Met. Soc. AIME* **233**, 180 (1965).
13. B. G. HYDE, E. E. GARVER, V. E. KUNTZ, AND L. EYRING, *J. Phys. Chem.* **69**, 1667 (1965).
14. J. W. CAHN, *Acta Met.* **4**, 449 (1956).
15. J. HASCHKE AND L. EYRING, *Inorg. Chem.* **10**, 2267 (1971).
16. J. A. POULIS, "Vacuum Microbalance Techniques," Vol. 3, p. 1, Plenum, New York (1963).
17. D. R. KNITTEL, S. P. PACK, H. INABA, S. H. LIN, AND L. EYRING, unpublished material, available upon request from S. H. Lin.
18. L. EYRING, C. C. HERRICK, M. S. JENKINS, D. L. FOX, R. P. TURCOTTE, AND G. R. WEBER, Report No. C00-1109-46, p. 102 (1969).
19. C. N. R. RAO AND G. V. S. RAO, in "Proceedings, 8th Rare Earth Research Conference," Vol. 1, p. 345 (1970).
20. K. H. LAU, D. L. FOX, S. H. LIN, AND L. EYRING, *High Temp. Sci.* **8**, 129 (1976).
21. R. E. CARTER, *J. Chem. Phys.* **34**, 2010 (1961).
22. W. E. BOGGS, R. H. KACHIK, AND G. E. PELLISSIER, *J. Electrochem. Soc.* **112**, 539 (1965).
23. K. NAITO, N. KAMEGASHIRA, S. TAKEDA, AND T. KONDO, *J. Nucl. Sci. Technol.* **13(5)**, 260 (1976).